Hindawi
Geofluids
Volume 2020, Article ID 8728432, 18 pages
https://doi.org/10.1155/2020/8728432

Research Article

Diagenesis and Origination of Carbonate Cements in Deeply Buried Sandstones of the Eocene Es_3 Member, Raoyang Sag, Bohai Bay Basin, China

Kaixun Zhang,[1,2] **Xinxin Fang**,[1,2] **Ying Xie**,[3] **Shun Guo**,[4] **Zhenwang Liu**,[5] **and Lei Wang**[3]

[1]*Institute of Geomechanics, Chinese Academy of Geological Sciences, Beijing 100081, China*
[2]*Key Laboratory of Paleomagnetism and Tectonic Reconstruction, Ministry of Natural Resources, Beijing 100081, China*
[3]*PetroChina Huabei Oilfield Company, Renqiu, Hebei 062552, China*
[4]*Shaanxi Yanchang Petroleum (Group) Corp. Ltd., Xi'an, Shaanxi 710075, China*
[5]*Beijing Chengkaidelin Science & Technology Corp. Ltd., Beijing 102200, China*

Correspondence should be addressed to Xinxin Fang; 38530324@qq.com

Received 30 January 2020; Revised 14 September 2020; Accepted 17 October 2020; Published 20 November 2020

Academic Editor: Ricardo L. Silva

Diagenesis is one of the most predominant factors controlling reservoir quality in the deeply buried siliciclastic sandstones of the third member in the Eocene Shahejie Formation (Es_3), in the Raoyang Sag, the Bohai Bay Basin. In this study, thin section, cathodoluminescence (CL), scanning electron microscope (SEM), X-ray diffraction (XRD), Raman spectrum, carbon and oxygen isotopes, and fluid inclusion analyses are used to restructure paragenetic sequences and detect origins of carbonate cements recorded in this deeply buried member. Based on petrographic analyses, the Es_3 sandstones are identified as lithic arkoses and feldspathic litharenites at present, but derived from original arkoses and lithic arkoses, respectively. Geohistorically, the Es_3 sandstones have undergone two diagenetic episodes of eogenesis and mesogenesis. Events observed during eogenesis include chemical compaction, leaching of feldspar, development of chlorite coating and kaolinite, precipitation of the first generation of quartz overgrowth (QogI), dissolution of feldspar, and precipitation of calcite and nonferroan dolomite cement. Mesogenetic alterations include chemical compaction, precipitation of kaolinite aggregate and the second generation of quartz overgrowth (QogII), precipitation of ankerite, development of I/S and illite, and formation of pyrite. Carbon and oxygen isotopic data show that calcite cements are characterized by ^{13}C ($\delta^{13}C_{PDB}$ ranging from -0.7‰ to 1.0‰ with an average of 0.1‰) and ^{18}O ($\delta^{18}O_{SMOW}$ varying from 12.3‰ to 19.0‰ with an average of 16.2‰); these stable isotopic data combined with Z value (from 114.69 to 122.18) indicate skeletal debris ($\delta^{13}C_{PDB}$ ranging from -1.2‰ to -1.1‰ with an average of -1.15‰; $\delta^{18}O_{SMOW}$ varying from 23.0‰ to 23.2‰ with an average of 23.1‰) and ooids in adjacent carbonate beds involved in meteoric water and seawater from outside jointly served as the carbon sources. For nonferroan dolomite, the $\delta^{13}C_{PDB}$ value of -4.1‰ is a little bit negative than the calcite, and the $\delta^{18}O_{SMOW}$ of 14.3‰ is coincident with the calcite, which suggest the nonferroan dolomites come from the diagenetic fluids with a similar oxygen isotopic composition to that of the calcite but modified by the external acidic $\delta^{13}C$-depleted water. However, the ankerites are actually rich in ^{12}C ($\delta^{13}C_{PDB}$ ranging from -10.0‰ to -1.2‰, mean = −4.3‰) and ^{16}O ($\delta^{18}O_{SMOW}$ varying from 10.1‰ to 19.4‰, mean = 14.9‰), when combined with the distribution of cutting down along the direction pointing to sand-body center from the margin and microthermometric temperature (Th's) data mainly varying between 115.2°C and 135.5°C with an average of 96.0°C, indicating the main origination from the Es_3 source rocks with effective feldspar buffer action for the acidic fluids in the margins of the Es_3 sandstones. In addition, the necessary elements for ankerite such as Fe^{2+}, Ca^{2+}, and Mg^{2+} ions also come from organic matter and clay minerals during thermal maturation of the Es_3 source rocks. The study provides insights into diagenetic processes and origination of carbonate cements in the Es_3 sandstones; it will facilitate the cognition of predictive models of deeply buried sandstone reservoirs to some extent, which can reduce the risks involved in oil and gas exploration and development.

1. Introduction

As hydrocarbon exploration and development expand into technically difficult areas, deeply buried reservoirs have become even more important in recent years [1]. Under these circumstances, diagenesis, especially of deeply buried sandstones, is increasingly considered by geologists as one of the most essential factors controlling the quality of oil and gas reservoir through destroying, enhancing, or preserving porosity and permeability by means of various diagenetic mechanisms [2–9]. Indeed, the study of diagenetic processes based on identifying diagenetic events and paragenetic sequences, which is essential for the understanding and prediction of reservoir quality, not only contributes to enhancing the efficiency of hydrocarbon exploration but also promotes the yields of commercial development [5, 8, 10–13]. Reservoir quality is dependent on both the original depositional environment and postdepositional diagenetic modifications, including physical, chemical, and biological processes, which vary with the pressure, temperature, chemistry of fluids, and framework grains related to the evolution history of sedimentary basin [8, 13–17]. For those deeply buried sandstone reservoirs undergoing complex postdepositional alterations, prediction of reservoir quality faced many more difficulties due to the intricate component transformations that are controlled by fluid-rock interaction [5, 18–22]. As deeply buried sandstones rich in more reactive grains have higher susceptibility to mechanical compaction and more potential cements, dating authigenic mineral is relatively easier to understand the processes and patterns of diagenetic events when combining with compacted features [23].

The third member of the Eocene Shahejie Formation (Es_3) at a deep burial depth (>3000 m) is one of the most important sandstone reservoirs in the Raoyang Sag, the Bohai Bay Basin. It is mainly made up of deltaic sandstones interbedded with mudstone and lacustrine carbonate rocks, being subjected to a high diagenetic degree. This is the reason why the Es_3 reservoir displays remarkable heterogeneity with porosity ranging from 3% to 25% and permeability ranging from 0.01 mD to 100 mD [24–26]. Previous studies from the literatures regarding the Shahejie Formation in Raoyang Sag showed that significant progress has been made in recent years for the successful application of sequence stratigraphy [25, 27, 28]. However, diagenetic evolution of the Es_3 sandstones and origins of carbonate cementations have not yet been clearly identified. There have been no systematic studies into the internal connection between the diagenetic alterations and reservoirs quality of the Es_3 sandstones as a whole. Nevertheless, various types of diagenetic textures and authigenic minerals are obviously present in these sandstone reservoirs, which provide a large amount of information to reveal the spatial and temporal distribution of diagenesis, and enable paragenetic sequences to be assessed [22, 25, 29, 30].

In order to acquire an in-depth and detailed understanding for the key controlling factors of diagenesis and the origins of carbonate cements during and after deposition, a comprehensive, multitechnique approach of quantitative petrographic, mineralogy, fluid inclusion, Raman spectrum, and stable isotope analysis was used. This paper specifically seeks to address the following objectives:

(1) To better identify petrological characteristics and diagenetic types of the Es_3 member in Raoyang Sag, Bohai Bay Basin

(2) To reconstruct the paragenetic sequence of multiple diagenetic events in order to learn the diagenetic history

(3) To investigate the originations of the carbonate cements abundant in the Es_3 sandstones

2. Geological Setting

The Bohai Bay Basin, located in the east of China, is one of the most prolific petroliferous basins, covering a region of approximate 210,000 km^2 [29, 31, 32]. Structurally, it is bounded by the Jiaodong uplift to the east, the Taihang Mountains to the west, the Luxi uplift to the south, and the Yanshan Mountains and fold belt to the north [29, 33]. This basin, which formed on the North China platform from the early Tertiary to the Late Jurassic epoch, is a Cenozoic rift lacustrine basin, including six depressions as follows: Linqing, Jiyang, Bozhong, Jizhong, Huanghua, and Liaohe [27, 29, 31] (Figure 1). The tectonic evolution of the basin experienced two major stages, the syn-rift stage from 65.0 Ma to 24.6 Ma, represented by a phase of extensional faulting, and the postrift stage from 24.6 Ma to the present day, represented by the stage of thermal subsidence modified by synchronous strike-slip deformation [29, 34–37]. The syn-rift sequences are composed of Kongdian (Ek), Shahejie, and Dongying (Ed) Formations, deposited in deltaic and lacustrine environments [33, 34, 38, 39]. The postrift sequences consist of the Neogene Guantao (Ng), Minghuazhen (Nm), and the Quaternary Pingyuan (Qp) Formations, which were mainly deposited in fluvial and shallow water delta environments [33, 39–41].

The Raoyang Sag is an interior tectonic unit, which is characterized by a series of normal faults, lying in the central and south Jizhong depression (Figure 1). It is a half-graben with several major boundary faults on the northeast side and stratigraphic onlaps toward the southwest slope [42–44]. The Eocene Shahejie Formation comprising the main source rocks, seal rocks and reservoir rocks, is divided into four members from top downwards which are named Es_1, Es_2, Es_3, and Es_4 (Figure 2) [25, 27, 31, 45]. Our interval of interest, the Es_3 member, is characterized by braid delta facies deposited in shallow to semideep lake environment [24, 27]. Braid channels, subaqueous distributary channels, and channel bays are the predominant microfacies [24, 25]. As a response, large-scale gray sandstones and siltstones intercalated with gray-green and purplish-red mudstones prevailed within Raoyang area [24, 28, 45]. The paleo-climate oscillated frequently between dry and wet in an overall arid to semiarid climatic setting during the depositional period of the Es_3 member, with a relative lake level slowly rising due to rapid subsidence of the basement [29].

3. Samples and Methods

A total of 112 core samples representative of the Es_3 sandstones were collected from 28 bore holes at the depths

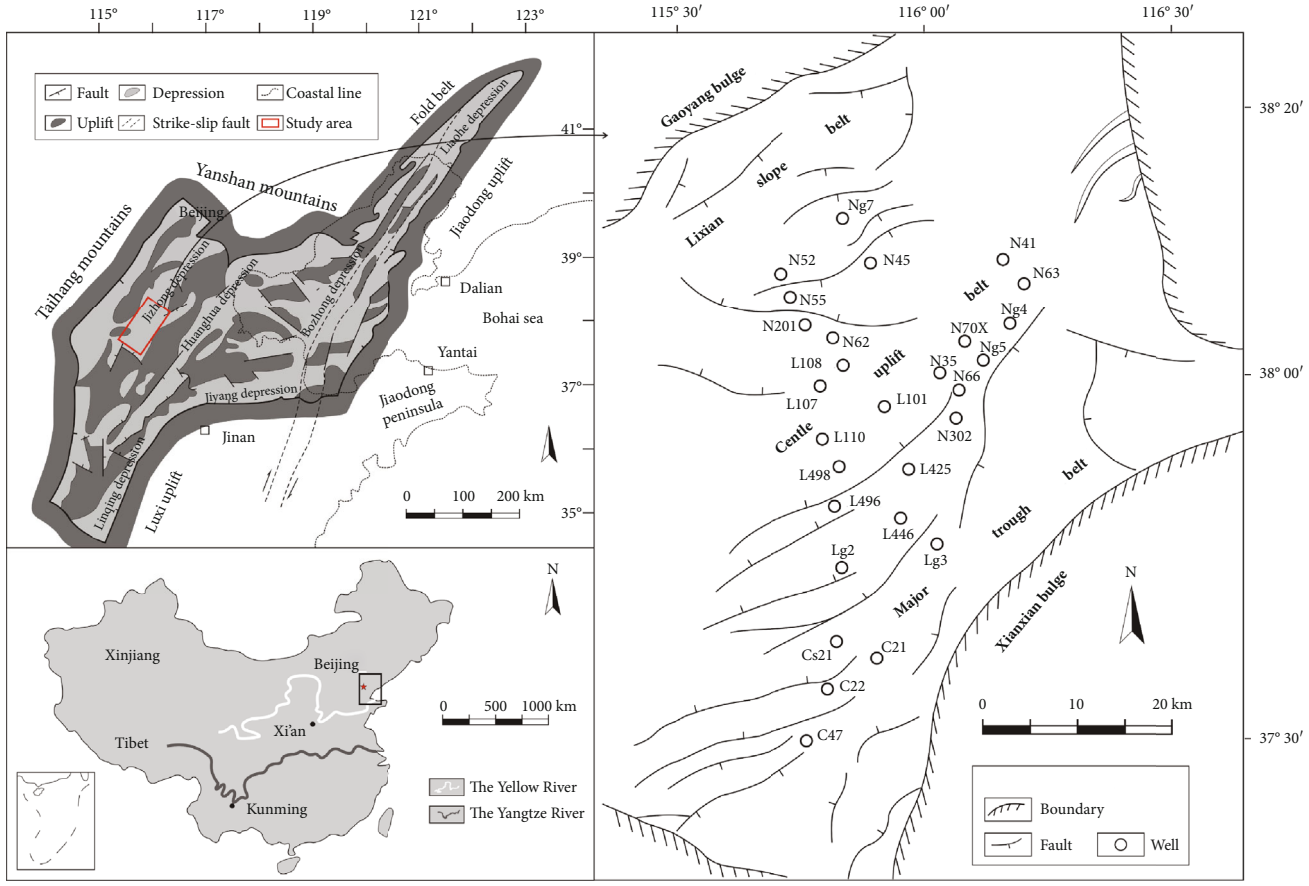

FIGURE 1: Tectonic setting of the Bohai Bay Basin, eastern China, and location map of the Raoyang Sag with its main structural features (modified from [29]).

ranging from 3100 m to 4800 m. All samples were impregnated with blue epoxy and stained with Alizarin Red S to help highlight pore textures and different types of carbonate minerals [46].

Petrographic examination was performed on all thin sections for each sample under a Nikon Eclipse E600POL microscope, and at least 300 points per thin section were counted for modal analysis. In addition, replaced and dissolved original components can be identified by optical characteristics of residue, residual shape, residual texture, etc. Cathodoluminescence (CL) was implemented on 35 uncovered thin sections by using a Leica DM2500 P cold cathodoluminoscope under standard operating conditions (16 kV accelerating voltage and 600 mA gun current).

In order to test the precipitation temperatures of cements, 25 doubly polished thin sections for microthermometric measurement were selected. Microthermometry was carried out by means of an Olympus BX-60 petrographic microscope equipped with a Linkam THMSG 600 heating and cooling stage. In addition, laser Raman spectrography was performed with a LabRAM HR800. Scanning electron microscope (SEM) at an acceleration voltage of 20 kV was carried out on 45 gold-coated samples to identify 3D textural relationships, especially clay minerals. Similarly, 45 samples were examined by X-ray diffraction (XRD) analyses of separated clay-sized particle fraction for identification of detrital components, cements, and various clay minerals.

Based on the identification of ankerite, calcite, and nonferroan dolomite by thin section observation, stable carbon and oxygen isotope testing of carbonate cements were performed on 22 samples. Sufficient powdered microsamples were treated with 100% H_3PO_4 at 50°C for 48 hours by using a MAT 251 isotope ratio mass spectrometer. The testing conditions and steps can refer to the literature by Swart et al. [47].

4. Results

4.1. Sandstone Texture and Compositions. According to thin section and SEM observations, the Es_3 reservoirs consist of fine to medium grained sandstones, with a grain size from 0.04 to 0.33 mm, but predominantly medium grained sandstones (Figures 3(a) and 3(b)). Under microscope, most of the detrital grains exhibit poorly to moderately sorted, subangular to subrounded shapes (Figure 3(a)), presenting long and concave-convex contacts between different grains (Figure 3(b)). Generally, most of the samples are characterized by rigid components, except for a few rich in biotite, clay mineral, and soft rock fragment (Table 1). Overall, the Es_3

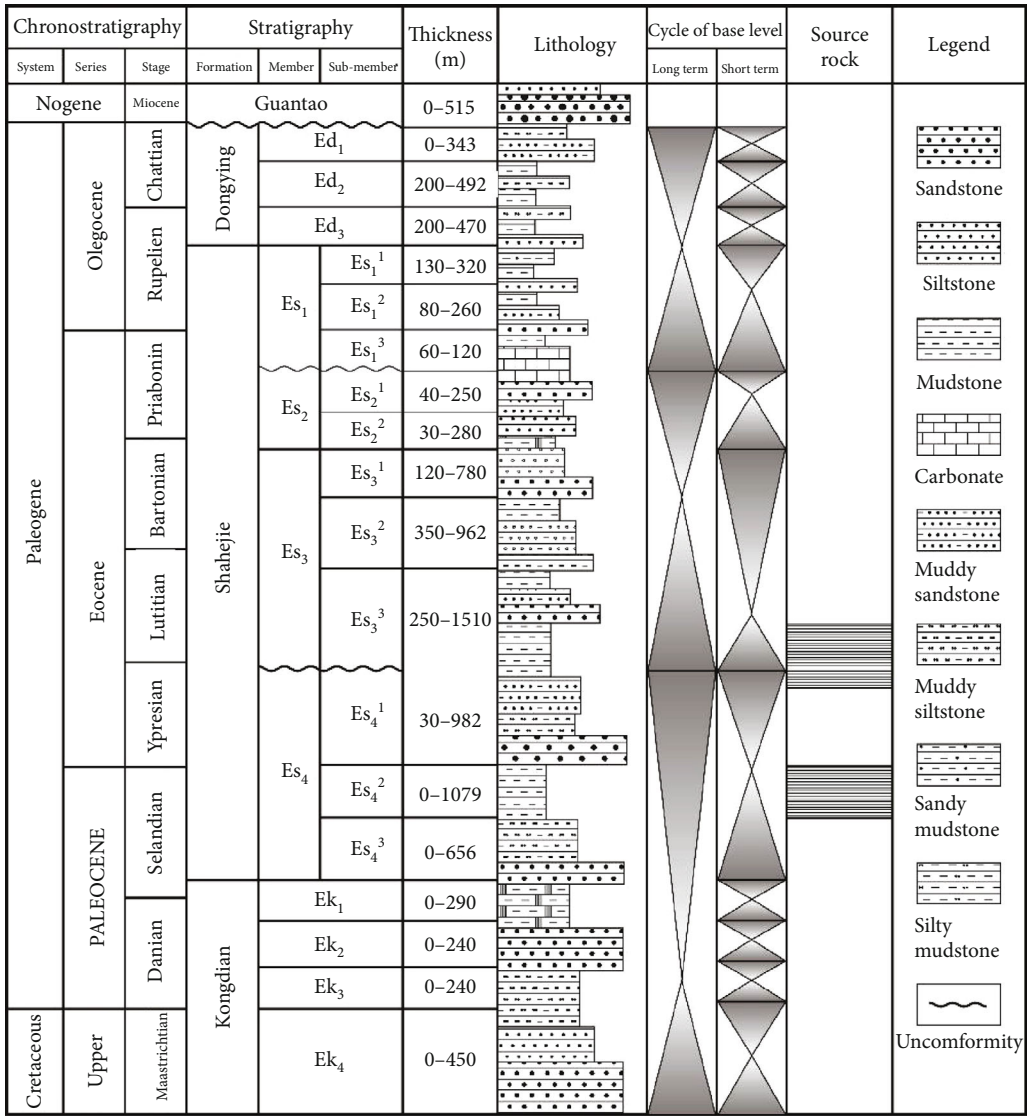

Figure 2: Regional composite lithostratigraphic column of the Raoyang Sag, with average thickness of the various stratigraphic units (modified from [25]).

sandstones are mineralogically immature with low to medium textural maturity (Figures 3(a), 3(b), and 3(g)).

Thin section point counting indicates that the framework grains of the Es_3 sandstones mainly comprise quartz, feldspar, rock fragment, and mica (Figure 3(c) and Table 1). Detrital quartz characterized by monocrystalline (av. 51.3% with min. 38.0% and max. 60.2%) captured numerous fluid inclusions and solid inclusions (Figure 3(d)), suggesting their origin of plutonic rocks. Polycrystalline quartz (Figure 3(d)) is much less common in content by contrast to the monocrystalline (av. 5.7% with min. 2.6% and max. 11.0%) (Table 1). In some cases, detrital quartz shows pitted and embayment-like margins engulfed strongly by carbonate cements (Figure 3(d), Figures 4(g) and 4(h)). Feldspar (Figures 3(e) and 3(f)) is another primary framework constituent, with plagioclases (av. 19.8%, min. 10.0% and max. 29.1%) quantitatively outnumbering K-feldspars (av. 5.1%, min. 2.0% and max. 11.0%) (Table 1). Microscopic investigation reveals an amount of feldspars are dissolved paralleling to the cleavage planes in parent grains under SEM (Figure 3(f)) and extensive carbonatization in plagioclases (Figures 3(b) and 3(d)). Due to the widespread carbonatization and dissolution, the abundance of original feldspars reduced dramatically (Table 1). Rock fragments in the Es_3 sandstones mainly derive from volcanic rocks (Figure 3(g)). So, volcanic rock fragment is much more than sedimentary and metamorphic counterpart in content (Table 1). According to point counting, the total contents of all types of rock fragments vary from 9.0% to 35.0% (av. 18.2%). Ooids and skeletal debris are rare (Figure 3(h)), ranging from 0.5% to 4.0% (av. 1.7%).

Owing to intensive dissolution (Figure 3(e)), replacement (Figure 4(f)), and cementation (Figure 4(a)) during burial, petrographic property has gradually changed with transformation in mineral content (Table 1). The present Es_3 sandstones are predominantly lithic arkoses

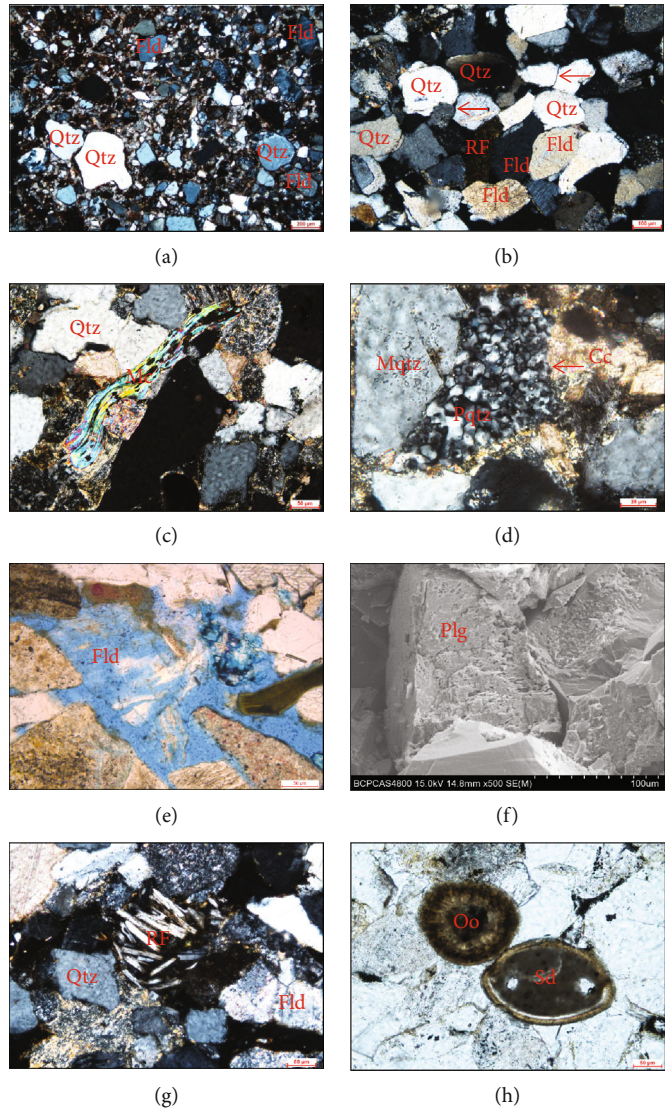

Figure 3: Lithological characteristics of the deeply buried Es_3 sandstones in Raoyang Sag. (a) Well NG7: 4077.3 m, fine to medium grained size with poor to moderate sorting, and subangular to subrounded grain shapes, XPL (crosspolarized light). (b) Well L101: 3705.8 m, rigid grains presenting long and concave-convex contact relations (arrow), XPL. (c) Well L425: 3668.2 m, mica containing ferruginous matters existing in samples, XPL. (d) Well L425: 3668.2 m, monocrystalline quartz containing numerous inclusions and bits of polycrystalline quartz (chert) engulfed by carbonate cementation (arrow), XPL. (e) Well N201: 3775.9 m, intensively dissolved feldspar, PPL (plane-polarized light). (f) Well N70X: 3566.3 m, feldspar dissolved along cleavages, SEM. (g) Well L101: 3796.0 m, andesite fragment rich in feldspar with pilotaxitic texture, XPL. (h) Well Ng7: 4077.3 m, ooids and skeletal debris with intact shapes, PPL. Qtz: quartz; Fld: feldspar; RF: rock fragment; Cc: carbonate cements; Mc: mica; Mqtz: monocrystalline quartz; Pqtz: polycrystalline quartz; Plg: plagioclase; Oo: ooid; Sd: skeletal debris.

and feldspathic litharenites based on composition point counting (Figure 5(a)). Actually, they, respectively, originated from arkose and lithic arkose when trace back to depositional time (Figure 5(b)) by the mean of distinguishing replaced and dissolved original minerals.

4.2. Diagenetic Minerals

4.2.1. Carbonate Cements. Carbonate cements are the most predominant authigenic minerals in the Es_3 sandstones (Figure 4(a)). Three types including ankerite, calcite, and dolomite were identified by using stained thin sections, CL, and X-ray analyses. Point counting data show ankerite abundance is much higher than the other carbonate cements, varying from 2.3% to 11.9% (av. 7.3%) (Table 1). These ankerites occur in the form of poikilotopic patches (Figures 4(a) and 4(d)) filling pore spaces and engulfing the margins of framework grains (Figure 4(d)) or early carbonate cements (Figure 4(e)). In some cases, detrital grains were replaced completely by these overgrown ankerites, so that those original components changed thoroughly as a result (Figure 4(f)). Calcite is subordinate to ankerite in content and ranges from 2.5% to 29.2% (av. 5.6%) (Table 1). Generally, it occurs as microcrystalline aggregate filling in

Table 1: Modal composition by point counting (%) for 15 samples from the deeply buried Es_3 sandstones.

Well no.	C_{22}		C_{s1}				L_{101}			L_{425}	L_{446}	L_{496}	N_{52}	N_{63}	Ng_5
Samples no.	C_{22-1}	C_{22-6}	Cs_{1-4}	Cs_{1-6}	L_{101-2}	L_{101-5}	L_{101-7}	L_{101-8}	L_{101-11}	L_{425-3}	L_{446-7}	L_{496-2}	N_{52-1}	N_{63-5}	Ng_{5-9}
Depth (m)	3855.9	4183.7	4297.22	4546.7	3619.0	3633.2	3644.1	3760.1	3786.6	3519.3	3593.4	3720.7	3536.4	3550.4	4756.9
S.d.m. face	B.c.	S.d.c.	S.d.c.	B.c.	B.c.	B.c.	B.c.	S.d.c.	S.d.c.	B.c.	S.d.c.	S.d.c.	B.c.	B.c.	B.c.
Detrital grains	59.2	62.5	56.9	64.3	61.6	63.4	56.3	67.0	59.7	62.3	61.3	55.6	58.9	43.9	53.5
Original quartz	60.0	65.0	63.0	49.0	59.0	61.0	58.0	53.0	57.0	59.0	65.0	50.0	58.0	62.0	59.0
Present quartz	58.0	63.0	62.0	54.0	58.0	60.0	55.0	52.0	62.0	56.0	64.0	49.0	48.0	55.0	58.0
Monocrystalline	49.5	56.3	59.4	47.3	49.6	55.1	49.7	49.2	58.5	51.2	60.2	38.0	44.5	48.3	52.2
Polycrystalline	8.5	6.7	2.6	6.7	8.4	4.9	5.3	2.8	3.5	4.8	3.8	11.0	3.5	6.7	5.8
Original feldspar	32.0	25.0	28.0	40.0	32.0	29.0	25.0	35.0	30.0	27.0	29.0	38.0	25.0	26.0	26.0
Present feldspar	27.0	20.0	23.0	36.0	33.0	28.0	20.0	34.0	26.0	15.0	26.0	39.0	17.0	17.0	12.0
Plagioclase	19.5	15.8	19.3	29.1	22.0	23.8	17.4	28.1	23.7	10.5	20.2	31.5	12.3	13.9	10.0
K-feldspar	7.5	4.2	3.7	6.9	11.0	4.2	2.6	5.9	2.3	4.5	5.8	7.5	4.7	3.1	2.0
Original R.f.	8.0	10.0	9.0	11.0	9.0	10.0	16.0	12.0	13.0	14.0	6.0	12.0	17.0	12.0	15.0
Present R.f.	15.0	17.0	15.0	10.0	9.0	12.0	25.0	14.0	12.0	29.0	10.0	12.0	35.0	28.0	30.0
Volcanic	9.5	10.0	80	6.0	6.0	10.0	20.0	9.0	8.0	20.0	8.0	9.0	28.0	20.0	20.0
Metamorphic	3.5	3.6	3.0	3.5	2.0	1.2	3.1	3.8	2.2	6.5	1.0	1.7	4.6	5.1	6.8
Sedimentary	2.0	3.4	2.0	0.5	1.0	0.8	1.9	1.2	1.8	2.5	1.0	1.3	2.4	2.9	3.2
Mica	1.5	1.0	1.5	2.0	1.5	1.5	2.5	0.5	3.0	5.0	1.5	0.5	1.0	2.5	1.5
Ooid and S.d.	1.5	0.5	1.0	0.5	1.0	0.5	5.0	0.5	1.0	2.0	2.5	1.5	3.0	4.0	0.5
Matrix	5.2	5.5	3.5	3.5	5.0	5.0	2.5	2.5	3.0	4.5	3.0	5.5	3.5	2.5	5.5
Au. minerals	22.1	20.4	22.8	18.2	20.6	19.6	21.5	17.5	21.8	15.4	20.2	26.8	24.1	39.0	30.2
Ankerite	8.9	7.5	6.0	6.6	6.0	6.8	7.0	5.5	9.5	5.4	6.7	11.9	7.8	2.3	11.3
Calcite	4.2	3.9	2.5	2.7	3.9	3.7	3.5	4.5	5.0	2.5	3.5	5.5	3.4	29.2	6.3
N.f. dolomite	2.8	1.5	2.2	1.5	2.5	2.8	2.0	1.5	2.0	2.0	1.5	2.7	2.1	1.5	2.5
Qog I	3.2	3.0	4.7	3.2	3.5	2.3	3.5	2.5	2.0	2.5	3.0	3.0	3.0	2.5	3.0
Qog II	1.5	2.1	3.2	1.2	2.5	2.0	1.5	1.5	1.0	1.0	1.0	1.0	2.0	1.5	1.5
Clay	1.0	1.9	3.2	2.5	1.2	1.5	3.5	1.0	3.2	1.5	3.5	2.2	4.7	1.5	4.3
Pyrite	0.5	0.5	1.0	0.5	1.0	0.5	0.5	0.5	0.1	0.5	1.0	0.5	1.1	0.5	1.3
Porosity	10.5	10.1	14.3	11.5	10.3	10.0	12.2	12.0	11.5	10.8	11.5	10.1	9.5	8.1	9.3

R.f.: rock fragment; S.d.: skeletal debris; Au.: authigenic; N.f.: nonferroan; S.d.m. face: sedimentary face; B.c.: brained channel; S.d.c.: subaqueous distributary channel.

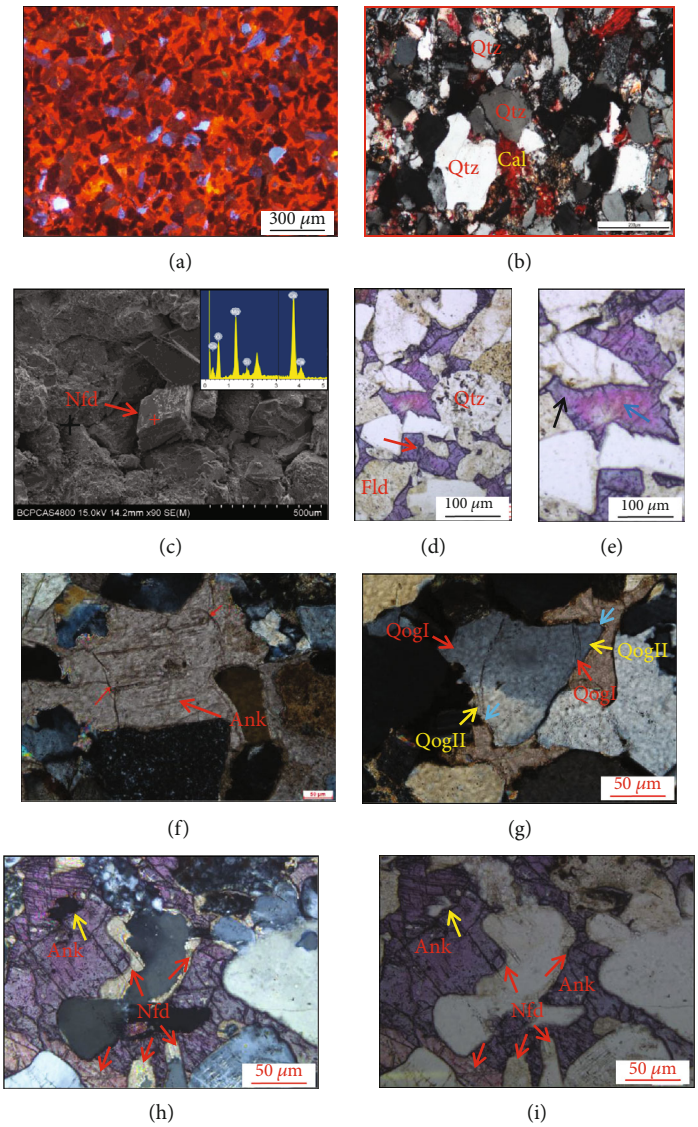

FIGURE 4: Diagenetic characteristics of the Es_3 sandstones in Raoyang Sag. (a) Well L101: 3644.7 m, a large deal of intergranular calcites acting as orange cathodoluminescence, CL. (b) Well N35: 3758.7 m, microcrystalline aggregates of calcite cements stained to be red, XPL. (c) Well NG4: 4680.0 m, rhombic euhedral nonferroan dolomite filling in intergranular pore, SEM. (d) Well L101: 3804.5 m, coarse-grained ankerites stained purple (red arrow) filling intergranular pores and replacing framework grains, PPL. (e) Well L101: 3804.5 m, late ankerite stained purple (black arrow) replacing early calcite stained red (red arrow), PPL. (f) Well L101: 3804.5 m, ankerite cements replacing original quartz grain completely, XPL. (g) Well L101: 3804.20 m, two generations of quartz overgrowths developed around detrital quartz grain, QogI (red arrow) developed continuously and QogII (yellow arrow) developed discontinuously, and engulfed by ankerite (blue arrow), meaning it is prior to ankerite, XPL. (h, i) Well C47: 3628.5 m, ankerite filling intergranular pores and replacing original quartz grains (yellow arrow), as well as nonferroan dolomite (red arrows) engulfing quartz grains, XPL and PPL. Cal: calcite; Ank: ankerite; Qtz: quartz; Nfd: nonferroan dolomite; QogI: the first generation of quartz overgrowths; QogII: the second generation of quartz overgrowths.

intergranular pores, which was stained dark red color in stained thin sections (Figure 4(b)). Rhombic nonferroan dolomite under SEM is rare (Table 1) and presents as scattered cements occluding primary pores or engulfing detrital grains (Figures 4(h) and 4(i)).

4.2.2. Quartz Cements. Authigenic quartz cements are mostly observed as syntaxial euhedral macrocrystalline overgrowths with a thickness from 5.0 to 62.0 μm around the detrital quartz grains in thin sections (Figure 4(g)), while prismatic outgrowths can easily be observed morphologically under SEM. Generally, linear fluid inclusion cluster and/or clay coatings near the grain margins are the signs for overgrowth and generation discrimination. There are two identified generations of the quartz overgrowths (Figure 4(g)). According to point counting, the first generation (QogI) is comparatively far more widespread (2.0% to 4.7% with an average of 3.0%) than those of the second generation (QogII) in coincidence with the content ranging from 1.0% to 3.2% with an average of 1.6% (Table 1). Thin sections show that QogI

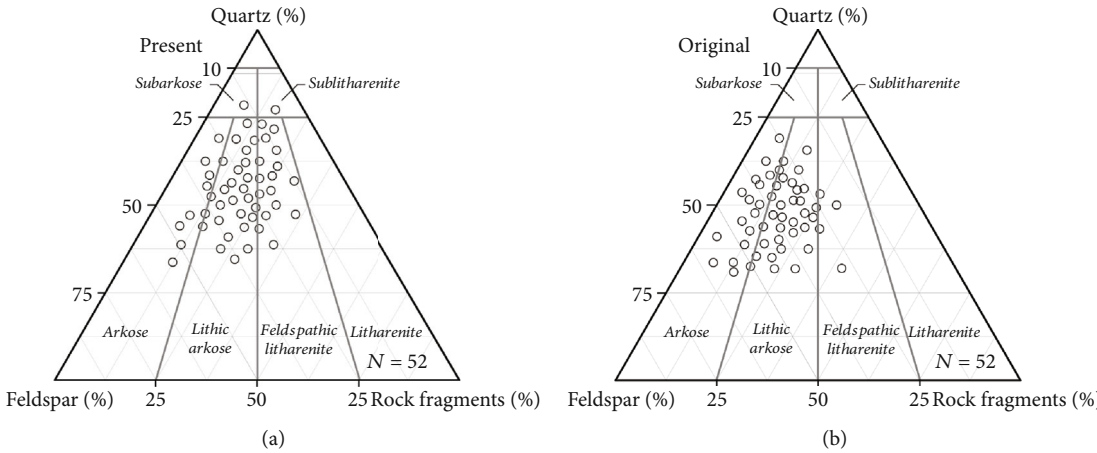

Figure 5: Present (a) and original (b) detrital compositions of the deeply buried Es_3 sandstones.

Table 2: X-ray diffraction of clay fractions in Es_3 member sandstones.

Well	Depth (m)	Sample no.	Kaolinite	Chlorite	Smectite	Illite	Mix-layered illite-smectite
C47	3627.4	Ch47-2	27.2	30.3	/	4.0	38.5
N70x	3565.9	N70x-8	49.1	16.5	/	4.2	30.2
Ng7	4078.0	Ng7-6	/	12.5	/	4.0	83.5
L101	3719.8	L101-5	/	44.3	/	5.5	50.2
L101	3643.6	L101-6	29.0	31.0	/	8.0	32.0
L101	3679.7	L101-9	/	/	/	2.6	97.4
N101	3775.9	N101-7	12.3	/	/	12.2	76.5
N35	3758.7	N35-2	11.1	/	/	6.3	82.6
N201	3547.8	N201-7	14.3	11.1	/	8.3	66.3
L107	3850.5	L107-3	12.2	14.4	/	6.5	66.9

prefers to develop continuously at the places where clay coatings are rare (Figure 4(g)). However, QogII usually developed discontinuously and intermittently.

4.2.3. Authigenic Clays. According to SEM morphologic characteristics combined with mineralogic analysis, there are four types of authigenic clay minerals (i.e., mix-layered illite/smectite, kaolinite, chlorite, and illite) developed in the Es_3 sandstones (Table 2 and Figure 6). Mix-layered illite/smectite (I/S), as an intermediate transformable product of smectite into illite, mainly takes the forms of foliage and/or honeycomb (Figure 7(a)). XRD indicates I/S occupies absolute dominance in total clay minerals with an average content of 62.4% (from 30.2% to 97.4%) (Table 2). Kaolinite is another prevailing mineral and occurs individually as pseudohexagonal euhedral crystal. There are two types of kaolinite developing in the samples according to occurrences, the one attaching to grain surfaces modified by pore fluids (Figure 7(b)) and the other one aggregating as clusters; kaolinite clusters often take the booklet-like or vermicular-stacked aggregate forms occluding pores near detrital feldspars (Figure 7(c)). Chlorite is also abundant in volume and its importance ought not be neglected. Generally, it develops in the form of rose-like sheaf, displays microcrystalline

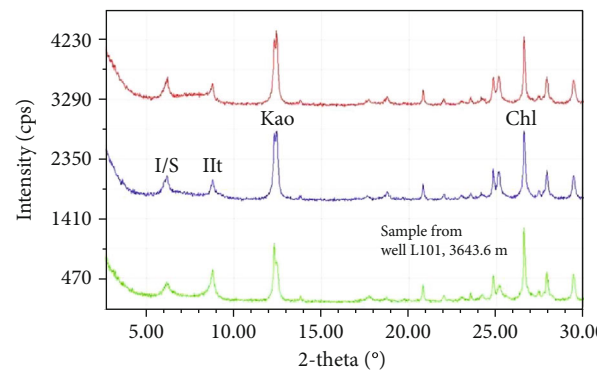

Figure 6: Representative clay fraction XRD spectra of the Es_3 sandstone reservoirs in Raoyang Sag. Kao: kaolinite; Ilt: illite; I/S: illite/smectite; Chl: chlorite.

habits, and covers on the grain surfaces acting as chlorite coatings (Figures 7(d) and 7(e)). Authigenic illite polytypes often occur as pore-bridging cements consisting of fibrous crystals with long axis perpendicular to grain surfaces. Fibrous illites often grow into pores and block pore throats resulting in a drastic reduction in permeability (Figure 7(f)).

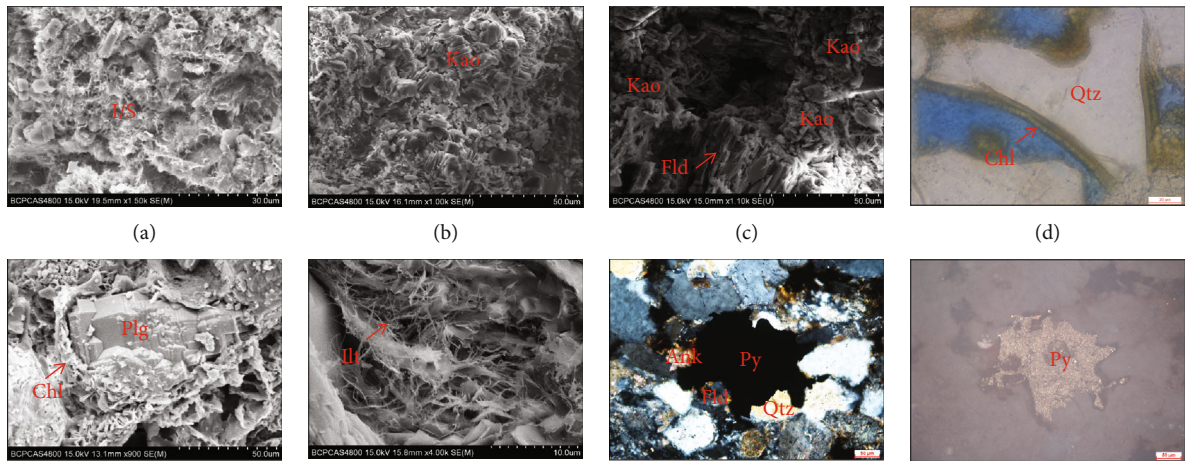

Figure 7: Diagenetic characteristics of the deeply buried Es_3 sandstones in Raoyang Sag. (a) Well LG3: 3824.3 m, I/S taking place as the forms of foliage and/or honeycomb, SEM. (b) Well L425: 3662.6 m, modified kaolinite to some extent attaching to grain surfaces, SEM. (c) Well N62: 3565.5 m, kaolinite aggregates developing in pores near dissolved feldspars, SEM. (d, e) Well N35: 3758.7 m, chlorite coating growing around framework grains, PPL and SEM. (f) Well L101: 3804.2 m, illite acting as fibrous crystals with long axis perpendicular to grain surfaces, XPL. (g, h) Well N35: 3758.72 m, pyrite engulfing and replacing quartz, feldspar, and ankerite, XPL and RL. I/S: illite/smectite; Kao: kaolinite; Plg: plagioclase; Fld: feldspar; Chl: chlorite; Py: pyrite; Qtz: quartz; Ilt: illite; RL: reflected light.

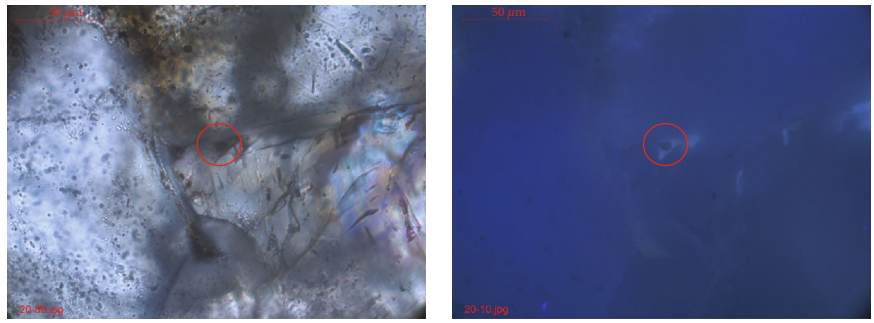

Figure 8: Photomicrograph of two-phase fluid inclusions in ankerite cement from the Es_3 sandstones under crosspolarized light (a) and fluorescent light (b).

4.2.4. Pyrite. Pyrite is traced in amount and distributes in examined samples as subregular patches (Figures 7(g) and 7(h)). It is easy to be identified in intergranular pores because of its characteristic for opaqueness to light. In thin sections, pyrite engulfs and thus postdates ankerite cements, implying its formation time of mesogenetic period.

4.3. Fluid Inclusion Analysis. Poikilotopic ankerite cements host a large deal of two-phase aqueous-dominated primary fluid inclusions with tiny gas bubbles (Figure 8). In addition, those inclusions are large enough with a size ranging from 2 to 16 μm for homogenization temperature (Th's) measurements. Microthermometric data shows that the ankerite cement Th's have an average of 96.0°C mainly varying between 115.2°C and 135.5°C (Figure 9).

4.4. Carbon and Oxygen Isotopic Composition. The data of carbon and oxygen isotope analysis on ankerite, calcite, and nonferroan dolomite cements are shown in Table 3 and Figure 10. For ankerite cement, $\delta^{13}C_{PDB}$ value varies between -10.0‰ and -1.2‰ with an average of -4.3‰ and $\delta^{18}O_{SMOW}$ value varies between 10.1‰ and 19.4‰ with average of 14.9‰. For calcite cement, $\delta^{13}C_{PDB}$ value ranges from -0.7‰ to 1.0‰ with an average of -0.1‰ and $\delta^{18}O_{SMOW}$ value ranges from 12.3‰ to 19.0‰ with average of 16.2‰. For nonferroan dolomite cement, $\delta^{13}C_{PDB}$ value is -4.1‰, and $\delta^{18}O_{SMOW}$ value is 14.3‰. For skeletal debris, $\delta^{13}C_{PDB}$ value varies between -1.2‰ and -1.1‰ with an average of -1.15‰ and $\delta^{18}O_{SMOW}$ value varies between 23.0‰ and 23.2‰ with average of 23.1‰.

5. Discussion

5.1. Diagenetic Events and Paragenetic Sequences. Diagenetic processes of the Es_3 sandstones have undergone two diagenetic stages: eogenesis (with maximum burial depth of 1.0-2.0 km and maximum temperature of 30-70°C, approximately) and

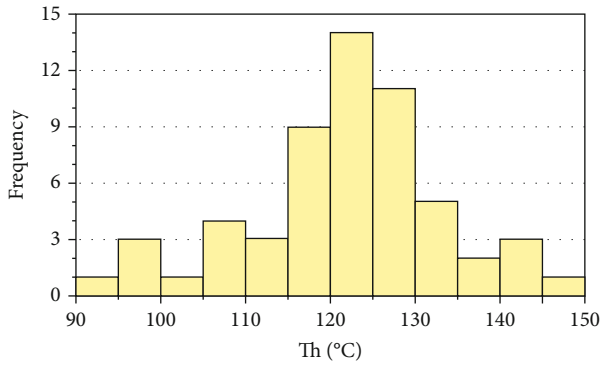

Figure 9: Histogram of homogenization temperatures (Th) from all primary fluid inclusions from the late ankerite cements in the Es_3 sandstones ($n = 57$).

mesogenesis (with burial depth deeper than 1.0-2.0 km and temperature higher than 30-70°C) [6, 13]. Actually, it is impossible to precisely measure absolute time and duration of each diagenetic event in detail. However, paragenetic sequences during burial can be reconstructed approximately by considering the diagenetic environments and mutual textural relations between authigenic components and/or initial constituents [23, 48].

5.1.1. Eogenetic Processes. Prior to becoming sedimentary rocks, all sediments had suffered diagenetic alterations at or near the surface of sediment pile, which is mainly influenced by the intergranular fluids deriving from depositional environment in an open system [6, 49]. First of all, mechanical compaction, which is more effective at packing loose sediments and driving intergranular water expulsion in initial burial stage, took place gradually in response to the increasing vertical stress [5, 6, 50]. Then, these sediments have been subjected to mechanical and chemical weathering alterations soon after deposition in the arid to semiarid climate during Es_3 period [26], which would inevitably lead to leaching of feldspar with respect to the flowing formation fluids by involving in infiltrated meteoric water [18, 51]. Petrographic observations show feldspars are often dissolved along cleavage significantly and thus create a mass of secondary pores (Figures 3(e) and 3(f)). At the same time, various authigenic clay minerals were produced, among which chlorite coatings formed firstly attaching to detrital grain surfaces, as there is not any other authigenic mineral existing in the space between the detrital grain and chlorite coating (Figure 7(d)), and mostly chlorite coatings contact directly with those detrital grains (Figure 7(e)). Additionally, these chlorite coatings not only protected original pores by enhancing the ability for resisting compaction but also served as barriers to retard the development of quartz overgrowths [49, 52]. Kaolinite is another important type of early clay mineral growing on the surfaces of detrital grains. Under SEM, these kaolinites had been modified with a low-level of euhedral texture (Figure 7(b)). Although these kaolinites were associated with feldspar leaching, yet they were removed timely and immediately in the flowing solution [30]. So, the random distribution of these kaolinites in samples was developed instead of concentrating in local position near secondary leaching pores [18, 30]. Except for early clay cements, calcite was a nonnegligible scenario in the eogenetic processes (Figure 4(b)). In some cases, those intergranular calcites characterized by fine microcrystal assemblage reach up to 29.2% in volume (Table 1 and Figure 4(a)). This is indicative of its early origin as only during the early stage of the eogenetic period can the sediments provide such spacious intergranular volumes for calcite development. On the other hand, these authigenic calcites directly cover the chlorite coatings or detrital grain surfaces in textural relations and thus postdate the authigenic chlorites (Figure 4(b)). In addition, a deal of well-preserved rather than dissolved ooids and skeletal debris were found out in thin sections (Figure 3(h)), which indicates that the patent water for calcite is rich in Ca^{2+} and CO_3^{2-} ions and thereby ensures the integrity of these ooids and skeletal debris. So, there exist material sources for early calcite precipitation [50, 53].

As the burial depth increases, the Es_3 sandstones entered in the late eogenetic field characterized by acidic environment [6]. In this stage, mudstone beds adjacent to the Es_3 sandstones began to generate and release organic acids by decarboxylation of organic matters due to a geotemperature close to 70°C [6, 25]. These processes not only led to secondary dissolution of feldspar but also resulted in early quartz cements [23]. Under microscope, there are abundant intragranular pores and/or even moldic pores evidencing the secondary dissolution of feldspar (Figure 3(f)). Unlike those early leaching-caused pores, these pores come with kaolinite aggregates close to dissolved feldspars (Figure 7(c)). From the perspective of porosity distribution, the ratio of secondary pores to the total pores is negatively correlated to the distance from the sand-body margin to center in individual sandstone near source rocks (Figure 11). This phenomenon indicates that the dissolving ability of organic acids gradually decreases with the increase in the distance between margin and center in individual sandstones [23, 50]. Dutton [53] documented feldspars had buffered acidic fluids and thus reduced solubility of Ca^{2+} irons and Mg^{2+} irons coming from adjacent source rocks, which resulted in nonferroan dolomite concentrated in sand-body margins.

According to Worden and Burley [6], twin characteristics of weak acidic environment and saturated SiO_2 produced by feldspar dissolution are conducive to the precipitation of quartz cements. As the Es_3 sandstones in the late eogenesis precisely met the above diagenetic environment conditions [25], the first generation of quartz cements (QogI) developed around protogenetic quartz grains as a response to the conditions and tended to take the forms of syntaxial euhedral overgrowths (Figure 4(g)) [6, 49]. With previous chlorite coatings having blocked, retarded, and even prevented nucleation for quartz growth, discrete overgrowths prevailed in the early stage and then interlocked with each other to form large overgrowths [52, 54].

5.1.2. Mesogenetic Processes. Mesogenetic events occur at a temperature higher than 70°C in Es_3 sandstones. These reactions include dissolution of feldspar, chemical compaction, formation of kaolinite aggregates, precipitation of the second

Table 3: Mineralogical and isotopic composition of carbonate cements, and calculated formation temperature of cements in the Es_3 sandstone reservoirs.

Wells	Depth (m)	Mineral types	Occurrence	Time	$\delta^{13}C_{PDB}$ (‰)	$\delta^{18}O_{PDB}$ (‰)	$\delta^{18}O_{SMOW}$ (‰)	Z value
C47	3627.40	Calcite	Microcrystalline	Early	1.0	-14.5	16.0	122.18
CS1	4293.68	Calcite	Microcrystalline	Early	0.1	-13.0	17.5	121.02
CS1	4540.81	Ankerite	Poikilotopic	Late	-1.2	-14.2	16.3	117.74
L101	3811.54	Ankerite	Poikilotopic	Early	-4.9	-17.9	12.5	108.57
L101	3782.26	Ankerite	Macrocrystalline	Late	-5.0	-17.2	13.2	108.51
L101	3757.18	Ankerite	Macrocrystalline	Late	-5.4	-17.4	13.0	107.58
L101	3633.18	N.f. dolomite	Macrocrystalline	Medium	-4.1	-16.1	14.3	110.87
L425	3693.75	Ankerite	Poikilotopic	Late	-5.2	-15.6	14.8	108.85
L425	3541.75	Ankerite	Poikilotopic	Late	-5.2	-15.6	15.9	108.85
L425	3599.10	Calcite	Poikilotopic	Early	-0.7	-18.1	12.3	116.78
NG5	4756.88	Calcite	Poikilotopic	Early	-0.6	-11.5	19.0	120.22
LG2	4250.34	Ankerite	Macrocrystalline	Late	-5.9	-17.8	12.0	106.26
C22	4117.46	Ankerite	Macrocrystalline	Late	-3.6	-12.7	17.8	113.55
N41	3522.12	Ankerite	Macrocrystalline	Late	-3.7	-14.8	15.6	112.27
N41	3507.43	Ankerite	Macrocrystalline	Late	-2.0	-12.8	17.8	116.89
N201	3547.78	Ankerite	Macrocrystalline	Late	-2.5	-15.0	15.4	121.16
N62	3565.50	Calcite	Poikilotopic	Early	-0.4	-14.3	16.1	114.69
N63	3548.71	Ankerite	Poikilotopic	Late	-1.9	-11.2	19.4	121.05
N70X	3566.32	Ankerite	Macrocrystalline	Late	-10.0	-15.4	15.1	119.34
N52	3539.30	Ankerite	Microcrystalline	Late	-3.5	-20.2	10.1	117.85
N35	3750.75	Bioclasts		Early	-1.1	-7.6	23.0	99.21
N201	3764.36	Bioclasts		Early	-1.2	-7.4	23.2	110.09

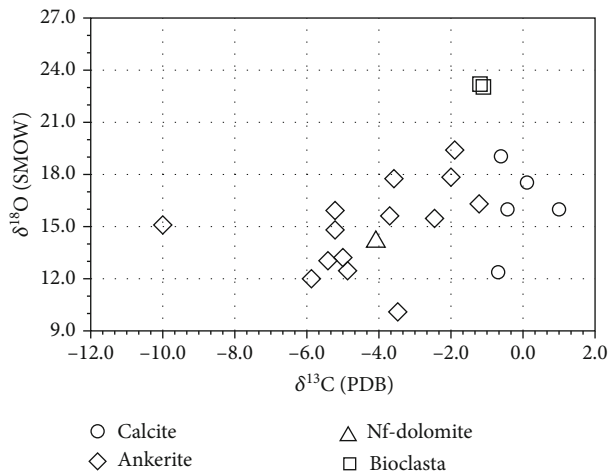

Figure 10: Distribution characteristics of carbon and oxygen isotopes for carbonate cements.

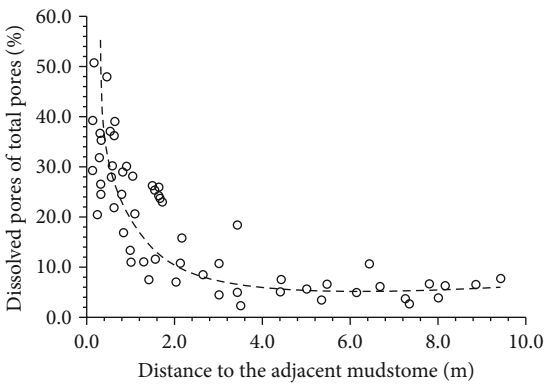

Figure 11: Distribution for the ratio of dissolved pores to total pores in individual sand-body deposited in brained channel with a thickness of 30.6 m versus the distance from test point to the contact interface between the sandstone and adjacent mudstone.

generation of quartz overgrowth (QogII), and ankerite development.

With the increase in burial and temperature, more and more organic acid and organic CO_2 from Es_3 source rocks by thermal decarboxylation of kerogen were released and injected into Es_3 sandstones. So, the dissolution of feldspar in the late stage of eogenesis continued to mesogenetic period. On the other hand, a series of long and concave-convex contacts between detrital quartz grains developed widely, representing the typical chemical compaction with progressive burial (Figure 3(b)) [7, 55]. In the meantime, mechanical compaction of the Es_3 sandstones turned gradually into weakened so that it had been subordinate to chemical compaction, which limited the liquidity of formation water and resulted in porosity reduction. And thus, a large amount of kaolinite aggregates coming from the locally supersaturated solution can only precipitate in the pore

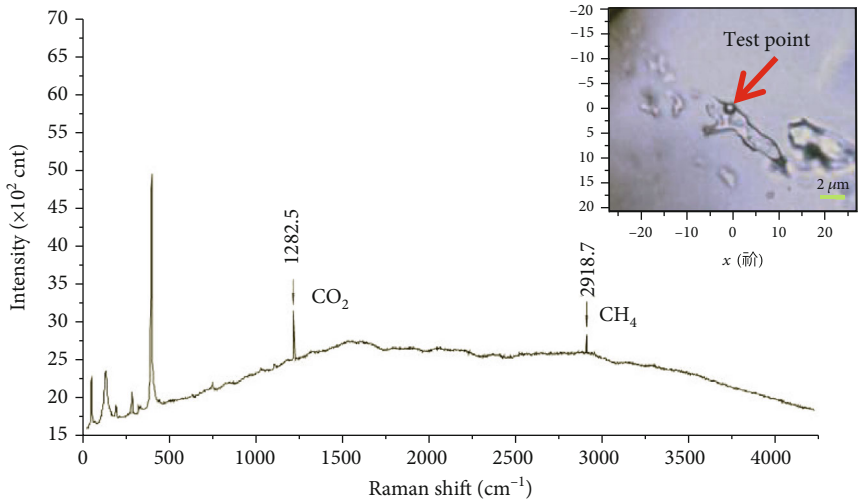

Figure 12: Laser Raman spectroscopy of fluid inclusions in quartz cements for the Es_3 member sandstones..

spaces near the dissolved feldspars (Figure 7(c)). Shelton [56] documented that kaolinite cements derived from crystallization of solution materials in pore water often precipitate as pore aggregates of infilling [57]. In addition, petrological observations show QogII developed around QogI and near concave-convex contacts (Figure 4(g)). Dissolution of feldspar and pressure solution of detrital quartz possibly account for SiO_2 sources to a large extent [57–60]. Texturally, these QogIIs also presented syntaxial texture in coincidence with the QogIs, but far less than QogIs in abundance (Table 1). In addition, the existence of CO_2 in formation water during the precipitation of QogIIs is proved by the fact that CO_2 was detected in fluid inclusions by laser Raman spectroscopy (Figure 12). This detection, therefore, suggests feldspar dissolution in the Es_3 sandstones indeed occurred in formation water containing both organic CO_2 and organic acids.

XRD shows mix-layered illite/smectite (I/S) is the most widespread clay minerals without smectite at all in the Es_3 sandstones (Table 2, Figure 6). According to previous studies, there are two mechanisms, transformation of kaolinite and replacement of smectite, for illite development [57, 60, 61]. However, kaolinite developed very well in the pore systems and no evidence indicates conversion of kaolinite to illite. On the contrary, smectite was not detected at all by XRD and SEM (Table 2, Figure 6), which probably imply that those smectites have transformed to illite and/or transitional product of I/S. Moreover, many literatures documented that transformation of smectite to illite can occur in the temperature environment of mesogenesis [60, 62]. In fact, smectite has not yet been fully converted into illite, but in the stage of I/S (Table 2). Morphologically, flaky occurrences of I/S (Figure 7(a)) and illite (Figure 7(f)) definitely support early smectite as precursor, which is coincident with mesogenetic condition during burial [60].

Quantitatively, blocky and poikilotopic ankerite is volumetrically predominated in Es_3 sandstones (Figure 4(d)), filling in remnant intergranular pores and intensely replacing original detrital quartz (Figure 4(f)), feldspar, and early calcite cement (Figure 4(e)) in situ. Texturally, these ankerites not only engulfed, and thus postdated the QogII (Figure 4(g)) [49, 63], but also replaced feldspar and quartz partly or completely, leading to oversized patches in some cases (Figure 4(f)). Fortunately, some original occurrences of those detrital grains were preserved to some extent. In addition, the Th's of two-phase fluid inclusions hosted in these ankerites concentrate in the range of 115.2°C to 130.5°C with an average of 96.0°C (Figure 9), which indicate the chronology for the mesogenesis [52, 64]. According to the preserved mineral remnants and textures, those strong replacements resulted directly in the change of lithologies from arkosic arenites and lithic arenites to subarkosic arenites and sublithic arenites, respectively (Figure 5). In addition, concomitants with replacement and dissolution of K-feldspar providing sufficient K^+ ions in pore water lead to smectite transformation during the process of illitization [6]. Theoretically, pyrite formation requires Fe^{2+} and S^- ions in a reducing environment (Figures 7(g) and 7(h)). The condition for ankerite can also satisfy the requirements for pyrite during the evolution of organic matter in mesogenetic time [65–67]. According to the analysis of diagenetic events, the paragenetic sequences of those Es_3 sandstones are reconstructed (Figure 13) as follows.

5.2. Origin of Carbonate Cements. There are many studies focusing on the originations of carbonate cements in the past decades [7, 30, 53, 68, 69]. In those studies, the internal and external were concluded on the sources of carbonate cements both in terrestrial and marine sandstones [53]. Internal sources include the initial carbonate rock fragments, ooids, and skeletal debris, dissolving and reprecipitating in the host sandstones [53, 67, 70]. External sources include interbedded mudstones, bioclast-rich beds, and adjacent source rocks, transporting into sandstones from outside [50, 53, 71–73].

Petrographic observations indicate a few of skeletal debris and ooids can be found out in the Es_3 sandstones (Figure 3(h)). However, the abundances of these components are too low in negligible quantity to supply such a large volume of carbonate cements (Table 1). There is rare

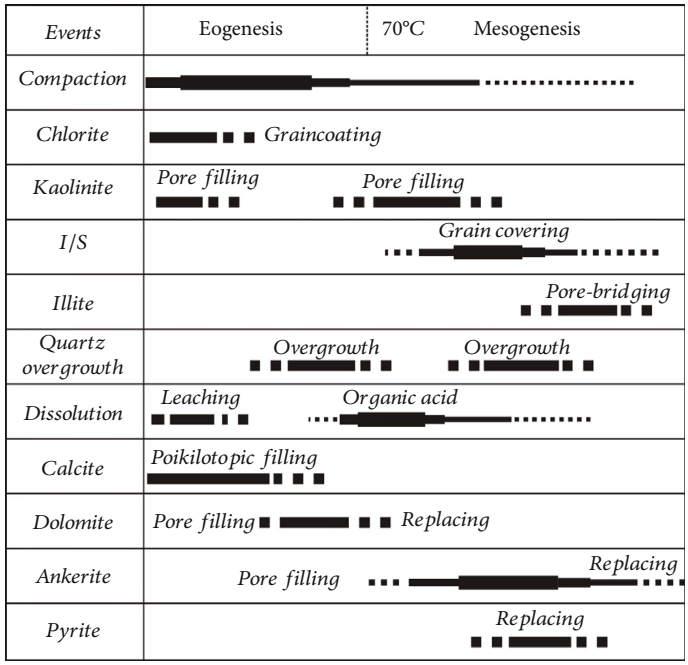

Figure 13: General paragenetic sequences of the Es_3 sandstones deeply buried sandstone in Raoyang Sag Bohai Bay Basin.

petrographic evidence showing that dissolution occurred in these ooids and thus not ruling out their possibilities as internal sources of carbonate cements [53]. Moreover, the positive correlation between the content of ooids and the content of total carbonate cements in the Es_3 sandstones (Figure 14) indeed indicates their importance for carbonate cements. Even if the total volume of secondary pores resulted from the dissolution of these internal carbonate constituents, it would not account for such a significant volume of carbonate cement. As a result, external source inputs are considered the principle origin of carbonate cements.

According to the existence of undissolved ooids and skeletal debris in samples (Figure 3(h)), we infer that the primary sedimentary water had a high-level concentration of Ca^{2+} and CO_3^{2-} (CO_2) ions. On the other hand, with the increase in temperature during burial, the solubility of $CaCO_3$ decreased as a response, which caused a constant imbalance in chemical equilibrium and thus resulted in a direct precipitation for early calcite cements from the pore water as an external source (Figures 4(a) and 4(b)). Regarding isotopic compositions, carbon isotopic data imply calcite cements derived from biogenic carbonate (Figure 10). The $\delta^{13}C_{PDB}$ value of calcites ranging from -0.7 to 1.0‰ in conjunction with the ooids and skeletal debris values of -1.2 and -1.1‰ (Table 3) indicates the main source of ooids and skeletal debris was modified by meteoric water for calcite cements [53, 74]. However, the skeletal debris and ooids that sourced the cement mainly come outside from the upper Es_3 member developing lacustrine carbonate strata rich in skeletal debris and ooids due to the abundance constraint in Es_3 sandstones [75, 76]. In addition, $\delta^{18}O_{SMOW}$ value of these calcites varies between 12.3‰ and 19.0‰—far less than the values of 23.0‰ and 23.2‰ for the skeletal debris (Table 3). But an average $\delta^{18}O_{SMOW}$ of -11.91‰ for the meteoric water has

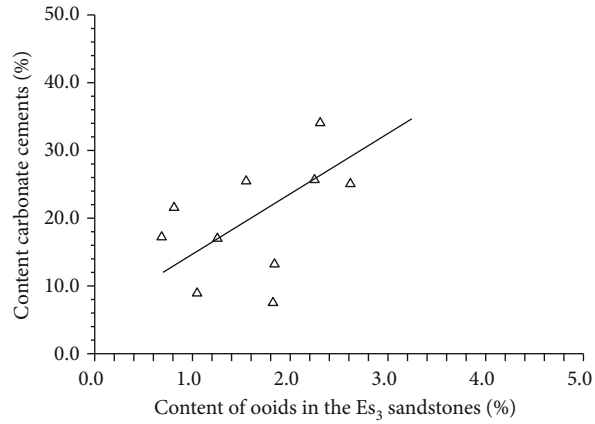

Figure 14: Relationship between content of carbonate cements and content of ooids in the Eocene Es_3 sandstones.

been estimated in previous study [77]. Thus, the skeletal debris, with a contribution of $\delta^{18}O$-depleted meteoric water, provide material sources for those early calcite cements which is consistent with the result by $\delta^{13}C$. Based on the empirical formula for determining marine limestone and freshwater limestone to Jurassic and younger strata proposed by Keith and Weber [78], the calculated Z value ranges from 114.69 to 122.18 with an average of 118.98 (Table 3). There are five Z values being more than 120 which indicate seawater has involved in the formation of calcite to a certain extent [79]. Therefore, the probable four sources including skeletal debris, ooids, meteoric water, and seawater jointly served as the originations for early calcite cements.

Owing to the low volume of nonferroan dolomite in the Es_3 sandstones (Table 1), it is hard to acquire adequate

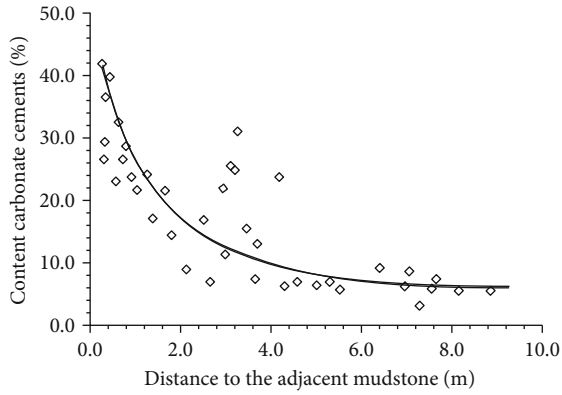

Figure 15: Distribution for the content of carbonate cements in individual sand-body deposited in brained channel with a thickness of 30.6 m versus the distance from test point to the contact interface between the sandstone and adjacent mudstone.

information for its origin. However, the $\delta^{13}C_{PDB}$ of -4.1‰ and $\delta^{18}O_{SMOW}$ of 14.3‰ (Table 3) likely suggest that the nonferroan dolomite cement precipitated from the liquids similar in oxygen isotopic composition to that of the calcite formation water but modified by the external acidic $\delta^{13}C$-depleted water during the late stage of eogenetic time [53]. When it comes to the extensively developed ankerites, distribution pattern of ankerite-cemented zones can reflect the source of ankerite from a macroscopic view to some extent [29]. Figure 15 shows that ankerite mainly concentrates in the margins of sand-bodies and gradually cuts down in the direction pointing to sand-body center. This distribution of ankerite suggests its origin from outside the Es_3 sandstones, with preferential development and cementation in the margins of sand-bodies.

From the perspective of stable isotope, the carbon and oxygen isotopic data obtained for ankerite cements are much lower than those for early calcite cements (Table 3). Experimentally, the $\delta^{13}C_{PDB}$ and $\delta^{18}O_{SMOW}$ of these $\delta^{13}C$-depleted ankerites in the Es_3 sandstones, respectively, range from -10.0‰ to -1.2‰ and 10.1‰ to 19.4‰ (Table 3). Liu et al. [68] claimed carbon isotope for carbonate cements in sandstone is more positive than those for their origin by 9.0‰ to 10.0‰ because of the carbon isotope fractionation in diagenetic processes. The relatively $\delta^{13}C$-depleted carbon for ankerites indicates an organic source from the decarboxylation of organic matter with a negative $\delta^{13}C$ down to -33.0‰ or -18.0‰ [68, 80]. In addition, the low $\delta^{18}O$ value for ankerite is still coincident with calcite precipitation from meteoric fluids, but formed at a much higher temperature in keeping with the microthermometric results upon gradually progressive burial. The Th's of the fluid inclusions in those authigenic ankerites concentrate in the range between 115.2°C and 135.5°C with an average of 96.0°C (Figure 9).

In terms of geochemical elements, such more ankerite cements certainly require an abundant supply for Fe^{2+} ions. However, dissolution of ferromagnesian grains and breakdown of volcanic rock fragments are insufficient to offer the large amount of Fe^{2+} ions needed for ankerites [81, 82]. Berner [83] documented that the concentration on iron and organic matter varied synchronously in fine deposits. The existence of largely organic OC-Fe (organic carbon associated with reactive iron phases) macromolecular structures tends to dissolve, and thus, those Fe^{2+} ions succeeded the parent body of source rocks during iron reduction process in reducing condition. Upon continual burial of the Es_3 source rocks containing a huge amount of organic matter, temperature increased gradually. So, adequate Fe^{2+} ion reserves were released into the formation water with the oxygen level in formation water becoming depleted [84]. In the meanwhile, with the alteration of clay minerals in source rocks as a response to the temperature increasing plus dissolution of ferromagnesian grains and volcanic rock fragments, Ca^{2+} and Mg^{2+} ions were offered for ankerite precipitation [48, 53, 57].

6. Conclusions

(1) The deeply burial Es_3 sandstones are mostly subangular-to-subrounded lithic arkoses and feldspathic litharenites with a fine to medium grain size and poor to moderate sorting, which were actually derived from arkoses and lithic arkoses, respectively

(2) The Es_3 sandstones have undergone two diagenetic episodes of eogenesis and mesogenesis. Eogenetic events that were identified include mechanical compaction, leaching of feldspar, development of chlorite coating and kaolinite, precipitation of the first generation of quartz overgrowth, dissolution of feldspar, and precipitation of calcite and nonferroan dolomite cement. Mesogenetic alterations include chemical compaction, precipitation of kaolinite aggregate and the second generation of quartz overgrowth, precipitation of ankerite, transformation of I/S and illite, and formation of pyrite

(3) Carbonate cements are the most major pore filling components. For calcite, skeletal debris and ooids in adjacent carbonate beds combined with meteoric water and seawater from outside jointly served as the carbon sources; for nonferroan dolomite, it directly precipitated in the diagenetic environment with oxygen isotopic composition similar to composition to that of the calcite but modified by the external acidic $\delta^{13}C$-depleted water; for the most widespread ankerite, it mainly originated from the Es_3 source rocks with effective feldspar buffer action for the acidic fluids along the margins of the Es_3 sandstones. In addition, the other necessary elements such as Fe^{2+}, Ca^{2+}, and Mg^{2+} ions also come from organic matter and clay minerals during thermal maturation of source rocks

Data Availability

The 112 core samples representative of the Es_3 member in the Raoyang Sag data used to support the findings of this study are included within the article.

Conflicts of Interest

The authors declare that they have no conflicts of interest.

Acknowledgments

We thank PetroChina Huabei Oilfield Company for providing samples and data access. This study is based on work carried out by a large group of participants and supported by the Science Foundation of Chinese Academy of Geological Sciences (grant No. JYYWF20181201) and the PetroChina Major Scientific and Technological Project Research and Application of Key Exploration and Development Technological for Sustainable and Stable Production in Huabei Oilfield (grant No. 2017E-15). A great appreciation is given to Nicole Holliday, who helped with the modification of this manuscript.

References

[1] R. Weibel, H. Friis, A. M. Kazerouni, J. B. Svendsen, J. Stokkendal, and M. L. K. Poulsen, "Development of early diagenetic silica and quartz morphologies – examples from the Siri Canyon, Danish North Sea," *Sedimentary Geology*, vol. 228, no. 3-4, pp. 151–170, 2010.

[2] S. N. Ehrenberg, "Preservation of anomalously high porosity in deeply buried sandstones by grain-coating chlorite: examples from the Norwegian Continental Shelf," *The American Association of Petroleum Geologists Bulletin*, vol. 77, pp. 1260–1286, 1993.

[3] M. J. J. Rahman and T. McCann, "Diagenetic history of the Surma Group sandstones (Miocene) in the Surma Basin, Bangladesh," *Journal of Asian Earth Sciences*, vol. 45, pp. 65–78, 2012.

[4] S. Stonecipher, R. Winn Jr., and M. Bishop, "Diagenesis of the frontier formation, Moxa Arch: a function of sandstone geometry, texture and composition, and fluid flux," *AAPG Bulletin*, vol. 68, pp. 289–316, 1984.

[5] T. R. Taylor, M. R. Giles, L. A. Hathon et al., "Sandstone diagenesis and reservoir quality prediction: models, myths, and reality," *AAPG Bulletin*, vol. 94, no. 8, pp. 1093–1132, 2010.

[6] R. Worden and S. Burley, "Sandstone diagenesis: the evolution of sand to stone," in *Sandstone Diagenesis*, Reprint Series 4 of the International Association of Sedimentologists, R. H. Worden, Ed., pp. 1–44, Blackwell Publishing, 2003.

[7] D. Xiong, K. Azmy, and N. J. F. Blamey, "Diagenesis and origin of calcite cement in the Flemish Pass Basin sandstone reservoir (Upper Jurassic): implications for porosity development," *Marine and Petroleum Geology*, vol. 70, pp. 93–118, 2016.

[8] Y. Zhou, Y. L. Ji, S. W. Zhang, and L. Wan, "Controls on reservoir quality of Lower Cretaceous tight sandstones in the Laiyang Sag, Jiaolai Basin, Eastern China: integrated sedimentologic, diagenetic and microfracturing data," *Marine and Petroleum Geology*, vol. 76, pp. 26–50, 2016.

[9] S. F. Zhu, Y. Jia, H. Cui et al., "Alteration and burial dolomitization of fine-grained, intermediate volcaniclastic rocks under saline-alkaline conditions: Bayindulan Sag in the Er'Lian Basin, China," *Marine and Petroleum Geology*, vol. 110, pp. 621–637, 2019.

[10] S. Bloch and K. P. Helmold, "Approaches to predicting reservoir quality in sandstones," *AAPG Bulletin*, vol. 79, pp. 97–114, 1995.

[11] S. Bloch, R. H. Lander, and L. Bonell, "Anomalously high porosity and permeability in deeply buried sandstones reservoirs: origin and predictability," *AAPG Bulletin*, vol. 86, no. 2, pp. 301–328, 2002.

[12] S. N. Ehrenberg, "Relationship between diagenesis and reservoir quality in sandstones of the Garn Formation, Haltenbanken, mid-Norwegian continental shelf," *AAPG Bulletin*, vol. 74, pp. 1538–1558, 1990.

[13] S. Morad, J. R. M. Ketzer, and L. F. de Ros, "Spatial and temporal distribution of diagenetic alterations in siliciclastic rocks: implications for mass transfer in sedimentary basins," *Sedimentology*, vol. 47, pp. 95–120, 2000.

[14] K. Bjørlykke, "Relationships between depositional environments, burial history and rock properties. Some principal aspects of diagenetic process in sedimentary basins," *Sedimentary Geology*, vol. 301, pp. 1–14, 2014.

[15] H. Mansurbeg, S. Morad, A. Salem et al., "Diagenesis and reservoir quality evolution of palaeocene deep-water, marine sandstones, the Shetland-Faroes Basin, British continental shelf," *Marine and Petroleum Geology*, vol. 25, no. 6, pp. 514–543, 2008.

[16] R. C. Surdam, "A new paradigm for gas exploration in anomalously pressured "tight gas sands" in the Rocky Mountain Laramide Basins," in *Seals, Traps, and the Petroleum System*, R. C. Surdam, Ed., vol. 67, pp. 283–298, AAPG Memoir, 1997.

[17] S. F. Zhu, K. Taylor, J. H. Chen, X. M. Zhu, S. Sun, and Y. Jia, "Controls on carbonate cementation in early syn-rift terrestrial siliciclastics: the Lower Cretaceous of the Bayindulan Sag in Er'lian Basin, China," *Marine and Petroleum Geology*, vol. 105, pp. 64–80, 2019.

[18] K. Bjørlykke and J. Jahren, "Open or closed geochemical systems during diagenesis in sedimentary basins: constraints on mass transfer during diagenesis and the prediction of porosity in sandstone and carbonate reservoirs," *AAPG Bulletin*, vol. 96, no. 12, pp. 2193–2214, 2012.

[19] J. G. Gluyas and T. Witton, "Poroperm prediction for wildcat exploration prospects: Miocene Epoch, Southern Red Sea," in *Reservoir Quality Prediction in Sandstones and Carbonates*, J. Kupecz, J. G. Gluyas, and S. Bloch, Eds., vol. 69, pp. 163–176, American Association of Petroleum Geologists Memoir, 1997.

[20] G. Thyne, "A model for diagenetic mass transfer between adjacent sandstone and shale," *Marine and Petroleum Geology*, vol. 18, no. 6, pp. 743–755, 2001.

[21] F. Tournier, M. Pagel, E. Portier, I. Wazir, and N. Fiet, "Relationship between deep diagenetic quartz cementation and sedimentary facies in a Late Ordovician glacial environment (Sbaa Basin, Algeria)," *Journal of Sedimentary Research*, vol. 80, no. 12, pp. 1068–1084, 2010.

[22] S. F. Zhu, X. X. Wang, Y. Qin et al., "Occurrence and origin of pore-lining chlorite and its effectiveness on preserving porosity in sandstone of the middle Yanchang Formation in the southwest Ordos Basin," *Applied Clay Science*, vol. 148, pp. 25–38, 2017.

[23] N. Molenaar, M. Felder, K. Bär, and A. E. Götz, "What classic greywacke (litharenite) can reveal about feldspar diagenesis: an example from Permian Rotliegend sandstone in Hessen, Germany," *Sedimentary Geology*, vol. 326, pp. 79–93, 2015.

[24] D. Z. Zhang, Y. L. Ji, and C. Y. Han, "Sedimentary characteristics and reservoir properties of the Shahejie Formation braided river delta in Raoyang Sag," *Geology in China*, vol. 36, no. 2, pp. 344–354, 2009.

[25] K. X. Zhang, G. P. Bai, F. M. Jin, and Q. Wang, "A sequence stratigraphy-based diagenetic study with the Sha-3 member sandstones in the central-south parts of the Raoyang depression as an example," *Acta Petrolei Sinica*, vol. 37, no. 6, pp. 728–742, 2016.

[26] D. J. Zou, X. H. Yu, and H. B. Liang, "Depositional system and sequence stratigraphy of third member of Shahejie Formation in Maxi Region, Raoyang Sag," *Natural Gas Geoscience*, vol. 19, no. 4, pp. 487–491, 2008.

[27] Y. L. Ji, J. H. Du, and X. Z. Zhao, "Sequence stratigraphy models and controlling factors of Eogene in Raoyang depression," *Acta Sedimentological Sinica*, vol. 25, no. 1, pp. 1–9, 2007.

[28] W. C. Zhang, Z. Q. Cui, C. Y. Han, and Y. J. Guo, "Evolution of Palaeogene lacustrine basins and oil and gas potentials in the central Hebei Depression," *Journal of Paleogeography*, vol. 1, pp. 45–54, 2001.

[29] J. Wang, Y. C. Cao, K. Y. Liu, J. Liu, X. Xue, and Q. Xu, "Pore fluid evolution, distribution and water-rock interactions of carbonate cements in red-bed sandstone reservoirs in the Dongying Depression, China," *Marine and Petroleum Geology*, vol. 72, pp. 279–294, 2016.

[30] S. F. Yang, Z. D. Bao, N. Wang et al., "Diagenetic evolution and its impact on reservoir quality of tight sandstones: a case study of the Triassic Chang 6 member, Ordos Basin, northwest China," *Marine and Petroleum Geology*, vol. 117, article 104360, 2020.

[31] Y. L. Feng, H. M. Zhou, and J. Y. Ren, "Paleogene sequence stratigraphy in the east of the Bohai Bay Basin and its response to structural movement (in Chinese)," *Scientia Sinica Terrae*, vol. 40, pp. 1356–1376, 2010.

[32] Z. X. Jiang and S. B. Xiao, "Hydrocarbon resource of the deep formation of Bohai Bay Basin," *Petroleum Explorationist*, vol. 1, pp. 16–19, 1998.

[33] C. Teng, F. Hao, H. Zou, X. Zhou, and C. Xu, "Tan-Lu fault system and its significance in oil accumulation in the central Liaodong Bay subbasin, Bohai Bay Basin, China," *AAPG Bulletin*, vol. 100, no. 2, pp. 289–314, 2016.

[34] M. B. Allen, D. I. M. Macdonald, Z. Xun, S. J. Vincent, and C. Brouet-Menzies, "Early Cenozoic two-phase extension and late Cenozoic thermal subsidence and inversion of the Bohai Basin, northern China," *Marine and Petroleum Geology*, vol. 14, no. 7-8, pp. 951–972, 1997.

[35] L. Y. Hsiao, S. A. Graham, and N. Tilander, "Seismic reflection imaging of a major strike-slip fault zone in a rift system: Paleogene structure and evolution of the Tan-Lu fault system, Liaodong Bay, Bohai, offshore China," *AAPG Bulletin*, vol. 88, no. 1, pp. 71–97, 2004.

[36] C. Lampe, G. Song, L. Cong, and X. Mu, "Fault control on hydrocarbon migration and accumulation in the tertiary Dongying depression, Bohai Basin, China," *AAPG Bulletin*, vol. 96, no. 6, pp. 983–1000, 2012.

[37] J. Qi and Q. Yang, "Cenozoic structural deformation and dynamic processes of the Bohai Bay basin province, China," *Marine and Petroleum Geology*, vol. 27, no. 4, pp. 757–771, 2010.

[38] Y. H. Deng, "Practical effect of the "transfer station" model for oil-gas migration in rift basin: a case study on the Tertiary in the Bohai oil province," *Acta Petrolei Sinica*, vol. 33, no. 1, pp. 18–24, 2012.

[39] Y. Yang and T. Xu, "Hydrocarbon habitat of the offshore Bohai Basin, China," *Marine and Petroleum Geology*, vol. 21, no. 6, pp. 691–708, 2004.

[40] Z. S. Gong, W. L. Zhu, and P. P. Chen, "Revitalization of a mature oil-bearing basin by a paradigm shift in the exploration concept. A case history of Bohai Bay, offshore China," *Marine and Petroleum Geology*, vol. 27, no. 5, pp. 1011–1027, 2010.

[41] F. Hao, X. H. Zhou, Y. Zhu, X. Bao, and Y. Yang, "Charging of the Neogene Penglai 19-3 field, Bohai Bay Basin, China: oil accumulation in a young trap in an active fault zone," *AAPG Bulletin*, vol. 93, no. 2, pp. 155–179, 2009.

[42] L. J. Tang, G. M. Wan, X. H. Zhou, W. Z. Jin, and Y. Y. Yu, *Cenozoic geotectonic evolution of the Bohai Basin (in Chinese)*, vol. 14, Geological Journal of China Universities, 2008.

[43] H. Zeng, X. Zhao, X. Zhu et al., "Seismic sedimentology of subclinoformal shallow-water meandering river delta: a case from the Suning area of Raoyang sag in Jizhong depression, Bohai Bay Basin, NE China," *Petroleum Exploration and Development*, vol. 42, no. 5, pp. 621–632, 2015.

[44] C. G. Zhang, "Tectonic framework and prolific hydrocarbon depressions in Bohai Bay: China offshore oil and gas," *Geology*, vol. 14, pp. 93–99, 2000.

[45] F. G. He, X. Z. Gao, X. Z. Zhao et al., "The lower part of the first member of the Shahejie formation (Es1x) as a source rock for oil found in Lixian Slope, Raoyang Sag, Bohai Bay Basin, Northern China," *Arabian Journal of Geosciences*, vol. 10, no. 5, 2017.

[46] J. A. D. Dickson, "Carbonate identification and genesis as revealed by staining," *SEPM Journal of Sedimentary Research*, vol. 36, pp. 107–118, 1966.

[47] P. K. Swart, S. Burns, and J. Leder, "Fractionation of the stable isotopes of oxygen and carbon in carbon dioxide during the reaction of calcite with phosphoric acid as a function of temperature and technique," *Chemical Geology: Isotope Geoscience section*, vol. 86, no. 2, pp. 89–96, 1991.

[48] A. D. S. G. Carvalho and L. F. De Ros, "Diagenesis of Aptian sandstones and conglomerates of the Campos Basin," *Journal of Petroleum Science and Engineering*, vol. 125, pp. 189–200, 2015.

[49] A. Pichat, G. Hoareau, J. P. Callot, and J. C. Ringenbach, "Diagenesis of Oligocene continental sandstones in salt-walled mini-basins–Sivas Basin, Turkey," *Sedimentary Geology*, vol. 339, pp. 13–31, 2016.

[50] M. J. J. Rahman and R. H. Worden, "Diagenesis and its impact on the reservoir quality of Miocene sandstones (Surma Group) from the Bengal Basin, Bangladesh," *Marine and Petroleum Geology*, vol. 77, pp. 898–915, 2016.

[51] O. S. Pokrovsky, S. V. Golubev, and J. Schott, "Dissolution kinetics of calcite, dolomite and magnesite at 25 °C and 0 to 50 atm pCO_2," *Chemical Geology*, vol. 217, no. 3-4, pp. 239–255, 2005.

[52] N. J. F. Blamey, K. Azmy, and U. Brand, "Provenance and burial history of cement in sandstones of the Northbrook Formation (Carboniferous), western Newfoundland, Canada: a geochemical investigation," *Sedimentary Geology*, vol. 299, pp. 30–41, 2014.

[53] S. P. Dutton, "Calcite cement in Permian deep-water sandstones, Delaware Basin, West Texas: origin, distribution, and

effect on reservoir properties," *AAPG Bulletin*, vol. 92, no. 6, pp. 765–787, 2008.

[54] E. D. Pittman, "Diagenesis of quartz in sandstones as revealed by scanning electron microscopy," *SEPM Journal of Sedimentary Research*, vol. 42, pp. 507–519, 1972.

[55] J. Lai, G. Wang, Y. Ran, Z. Zhou, and Y. Cui, "Impact of diagenesis on the reservoir quality of tight oil sandstones: the case of Upper Triassic Yanchang Formation Chang 7 oil layers in Ordos Basin, China," *Journal of Petroleum Science and Engineering*, vol. 145, pp. 54–65, 2016.

[56] J. W. Shelton, "Authigenic kaolinite in sandstone," *SEPM Journal of Sedimentary Research*, vol. 34, pp. 102–111, 1964.

[57] A. G. Oluwadebi, K. G. Taylor, and P. J. Dowey, "Diagenetic controls on the reservoir quality of the tight gas Collyhurst Sandstone Formation, Lower Permian, East Irish Sea Basin, United Kingdom," *Sedimentary Geology*, vol. 371, pp. 55–74, 2018.

[58] N. M. al Areeq, M. A. Soliman, M. A. Essa, and N. A. al-Azazi, "Diagenesis and reservoir quality analysis in the Lower Cretaceous Qishn sandstones from Masila oilfields in the Sayun-Masila Basin, eastern Yemen," *Geological Journal*, vol. 51, no. 3, pp. 405–420, 2016.

[59] O. Walderhaug, "Kinetic modeling of quartz cementation and porosity loss in deeply buried sandstone reservoirs," *American Association of Petroleum Geologists Bulletin*, vol. 80, pp. 731–745, 1996.

[60] R. H. Worden and S. Morad, "Quartz cementation in oil field sandstones: a review of the key Controversies," *Quartz Cementation in Sandstones*, vol. 29, pp. 1–20, 2000.

[61] V. Storvoll, K. Bjørlykke, D. Karlsen, and G. Saigal, "Porosity preservation in reservoir sandstones due to grain-coating illite: a study of the Jurassic Garn Formation from the Kristin and Lavrans fields, offshore Mid-Norway," *Marine and Petroleum Geology*, vol. 19, no. 6, pp. 767–781, 2002.

[62] M. D. Buatier, D. R. Peacor, and J. R. O'Neil, "Smectite-illite transition in Barbados accretionary wedge sediments: TEM and AEM evidence for dissolution/crystallization at low temperature," *Clays and Clay Minerals*, vol. 40, no. 1, pp. 65–80, 1992.

[63] A. M. Salem, S. Morad, L. F. Mato, and I. S. Al-Aasm, "Diagenesis and reservoir-quality evolution of fluvial sandstones during progressive burial and uplift: evidence from the Upper Jurassic Boipeba member, Reconcavo Basin, Northeastern Brazil," *AAPG Bulletin*, vol. 84, no. 7, pp. 1015–1040, 2000.

[64] K. Azmy, I. Knight, D. Lavoie, and G. Chi, "Origin of dolomites in the boat harbour dolomites of St. George Group, in western Newfoundland, Canada: implications for porosity development," *Bulletin of Canadian Petroleum Geology*, vol. 57, no. 1, pp. 81–104, 2009.

[65] K. Al-Ramadan, S. Morad, J. N. Proust, and I. Al-Aasm, "Distribution of diagenetic alterations in siliciclastic shoreface deposits within a sequence stratigraphic framework: evidence from the Upper Jurassic, Boulonnais, NW France," *Journal of Sedimentary Research*, vol. 75, no. 5, pp. 943–959, 2005.

[66] A. Karim, G. Pe-Piper, and D. J. W. Piper, "Controls on diagenesis of Lower Cretaceous reservoir sandstones in the western Sable Subbasin, offshore Nova Scotia," *Sedimentary Geology*, vol. 224, no. 1-4, pp. 65–83, 2010.

[67] S. Morad, "Carbonate cementation in sandstones: distribution patterns and geochemical evolution," in *Carbonate Cementation in Sandstones*, S. Morad, Ed., pp. 1–26, Blackwell Publishing Ltd., 1998.

[68] S. B. Liu, S. J. Huang, Z. M. Shen, Z. X. Lü, and C. R. Song, "Diagenetic fluid evolution and water-rock interaction model of carbonate cements in sandstone: an example from the reservoir sandstone of the fourth member of the Xujiahe Formation of the Xiaoquan-Fenggu area, Sichuan Province, China," *Science China Earth Sciences*, vol. 57, no. 5, pp. 1077–1092, 2014.

[69] C. L. Sombra and A. B. Barreto Jr., "Abstract: Stochastic Modeling of Calcite Concretions in Cretaceous Turbiditic Sandstones of the Albacora Oil-field, Campos Basin, Brazil," *AAPG Bulletin*, vol. 82 (1998), pp. 19–69, 1998.

[70] O. Walderhaug and P. A. Bjrkum, "Calcite growth in shallow marine sandstones: growth mechanisms and geometry," in *Carbonate cementation in sandstones*, S. Morad, Ed., vol. 26, pp. 179–192, Blackwell Publishing Ltd., 2009.

[71] P. S. Dutton and G. R. Loucks, "Diagenetic controls on evolution of porosity and permeability in lower Tertiary Wilcox sandstones from shallow to ultradeep (200–6700m) burial, Gulf of Mexico Basin, U.S.A," *Marine and Petroleum Geology*, vol. 27, no. 1, pp. 69–81, 2010.

[72] S. Gier, H. R. Worden, D. W. Johns, and H. Kurzweil, "Diagenesis and reservoir quality of Miocene sandstones in the Vienna Basin, Austria," *Marine and Petroleum Geology*, vol. 25, no. 8, pp. 681–695, 2008.

[73] K. L. Xi, Y. C. Cao, J. Jahren et al., "Diagenesis and reservoir quality of the Lower Cretaceous Quantou Formation tight sandstones in the southern Songliao Basin, China," *Sedimentary Geology*, vol. 330, pp. 90–107, 2015.

[74] M. G. Gross, "Variations in the O^{18}/O^{16} and C^{13}/C^{12} Ratios of diagenetically altered limestones in the Bermuda Islands," *Journal of Geology*, vol. 72, no. 2, pp. 170–194, 1964.

[75] Y. H. Du, "Eogene lacustrine carbonate rocks and sedimentary in Bohai Bay region," *Oil & Gas Geology*, vol. 11, no. 4, pp. 34–41, 1990.

[76] J. P. Yang, J. Yang, and A. J. Deng, "Carbonate rock facies model of the upper third member of Shahejie Formation of Paleogene in the central uplift belt of Raoyang Depression, Hebei Province," *Acta Sedimentologica Sinica*, vol. 28, no. 4, pp. 682–687, 2010.

[77] J. G. Ren, Y. P. Huang, and Z. S. Fang, "Oxygen and hydrogen isotope composition of meteoric water in the tropical West Pacific Ocean (in Chinese)," *Acta Oceanol. Sinica*, vol. 22, pp. 60–64, 2000.

[78] L. M. Keith and N. J. Weber, "Carbon and oxygen isotopic composition of selected limestones and fossils," *Geochimica et Cosmochimica Acta*, vol. 28, no. 10-11, pp. 1787–1816, 1964.

[79] W. F. Yuan, S. Y. Chen, and C. M. Zeng, "Research development and prospects on Paleogene sea transgression in Bohai Bay Basin," *Acta Sedimentologica Sinica*, vol. 4, pp. 7–16, 2005.

[80] G. H. Mack, D. R. Cole, T. H. Giordano, W. C. Schaal, and J. H. Barcelos, "Paleoclimatic controls on stable oxygen and carbon isotopes in caliche of the Abo Formation (Permian), South-Central New Mexico, U.S.A," *SEPM Journal of Sedimentary Research*, vol. 61, no. 4, pp. 458–472, 1991.

[81] I. C. Ryu and A. R. Niem, "Sandstone diagenesis, reservoir potential, and sequence stratigraphy of the Eocene Tyee Basin, Oregon," *Journal of Sedimentary Research*, vol. 69, no. 2, pp. 384–393, 1999.

[82] Z. Tang, J. Parnell, and A. H. Ruffell, "Deposition and diagenesis of the lacustrine-fluvial Cangfanggou Group (Uppermost

Permian to Lower Triassic), southern Junggar Basin, NW China: a contribution from sequence stratigraphy," *Journal of Paleolimnology*, vol. 11, no. 1, pp. 67–90, 1994.

[83] R. A. Berner, "Sedimentary pyrite formation," *American Journal of Science*, vol. 268, no. 1, pp. 1–23, 1970.

[84] K. Lalonde, A. Mucci, A. Ouellet, and Y. Gélinas, "Preservation of organic matter in sediments promoted by iron," *Nature*, vol. 483, no. 7388, pp. 198–200, 2012.